Magazine of Concrete Research, 2009, **61**, No. 9, November, 745–757
doi: 10.1680/macr.2008.61.9.745

The overlapping crack model for uniaxial and eccentric concrete compression tests

A. Carpinteri, M. Corrado, G. Mancini and M. Paggi

Politecnico di Torino

An analytical/numerical model, referred to as the overlapping crack model, is proposed in the present paper for the analysis of the mechanical behaviour of concrete in compression. Starting from the experimental evidence of strain localisation in uniaxial compression tests, the present model is based on a couple of constitutive laws for the description of the compression behaviour of concrete: a stress–strain law until the achievement of the compression strength and a stress–displacement relationship describing the post-peak softening behaviour. The displacement would correspond to a fictitious interpenetration and therefore the concept of overlapping crack in compression is analogous to the cohesive crack in tension. According to this approach, the slenderness and size-scale effects of concrete specimens tested under uniaxial compression are interpreted from an analytical point of view. Then, implementing the overlapping crack model into the finite element method, eccentric compression tests are numerically simulated and compared with experimental results. The influence of the size-scale, the specimen slenderness, as well as the degree of load eccentricity, is discussed in detail, quantifying the effect of each parameter on the ductility of concrete specimens.

Notation

b	thickness of the specimen
h	depth of the cross-section of the specimen
D_P	coefficient of influence for the applied force
$\{\boldsymbol{D}_w\}^{\mathrm{T}}$	vector of the coefficients of influence for the nodal displacements
e	load eccentricity
E	modulus of elasticity
E_{ci}	tangent modulus
E_{c1}	secant modulus from the origin to the peak compression stress σ_{c}
$\{\boldsymbol{F}\}$	vector of nodal forces
$\boldsymbol{F}_{\mathrm{c}}$	ultimate compression force
$\boldsymbol{F}_{\mathrm{u}}$	ultimate tensile force
G_{C}	crushing energy of confined concrete
$G_{\mathrm{C,0}}$	crushing energy of unconfined concrete
G_{F}	fracture energy
$\{\boldsymbol{K}_P\}$	vector of the coefficients of influence for the applied force
$[\mathbf{K}_w]$	matrix of the coefficients of influence for the nodal displacements
l	length of the specimen
P	applied force
$s_{\mathrm{E}}^{\mathrm{c}}$	brittleness number for plain concrete in compression
$\{\boldsymbol{w}\}$	vector of nodal displacements
w^{c}	overlapping displacements
$w_{\mathrm{cr}}^{\mathrm{c}}$	critical overlapping displacement
w^{t}	opening displacements
$w_{\mathrm{cr}}^{\mathrm{t}}$	critical crack opening displacement
δ	specimen shortening
$\boldsymbol{\varepsilon}$	strain
$\boldsymbol{\varepsilon}_{\mathrm{c}}$	strain at maximum load of $\boldsymbol{\sigma}-\varepsilon$ constitutive law
λ	slenderness of the specimen
ϑ	total rotation of the specimen
$\boldsymbol{\sigma}$	stress
$\boldsymbol{\sigma}_{\mathrm{c}}$	compression strength

Department of Structural Engineering and Geotechnics, Politecnico di Torino, Corso Duca degli Abruzzi 24, 10129, Torino, Italy.
(MACR 800120) Paper received 7 July 2008; last revised 20 February 2009; accepted 11 March 2009

Introduction

The compression behaviour of concrete, and in particular the ultimate strength and post-peak branch, have a predominant role in the design of concrete and concrete-based structures. Structural design, in fact, is usually conducted by comparing an action with a resistance evaluated on the basis of the ultimate strength. On the other hand, the post-peak behaviour is fundamental for a correct evaluation of the ductility, as, for

www.concrete-research.com 1751-763X (Online) 0024-9831 (Print)

example, for the evaluation of the ultimate axial deformation of columns or the rotational capacity of reinforced concrete (RC) beams. In this context, the size-scale effects play an important role, because the characteristic parameters of concrete are measured on specimens at a laboratory scale, that are far from the dimensions of a real structure. The problem of reduction of the compression strength by increasing the element size – the so-called size-effect – has been investigated in detail in the literature.[1,2]

The correct evaluation of the constitutive parameters is also complicated by many other testing aspects. The Round Robin programme carried out by the Reunion Internationale des Laboratoires et Experts des Materiaiux, Systemes de Construction et Ouvrages (RILEM) Technical Committee 148-SSC[3] demonstrated that the strength of concrete depends on the friction between the concrete and loading platen, as well as the slenderness of the specimen.[4] With decreasing slenderness, an increase of specimen strength is measured when rigid steel loading platens are used. However, when friction-reducing measures are used, for example by inserting a Teflon™ sheet between the steel loading platen and the concrete specimen, the compression strength measured on prisms or cylinders becomes almost independent of the slenderness ratio, l/h.[4,5] Moreover, the effect of friction disappears when the specimen slenderness is higher than 2·5. All the experiments of the aforementioned Round Robin programme revealed also that, in the softening regime, ductility (in terms of stress and strain) is a decreasing function of the slenderness. Furthermore, a close observation of the stress plotted against post-peak deformation curves showed that a strong localisation of deformations occurs in the softening regime, independently of the loading system, confirming the earlier results by van Mier.[6] The phenomenon of strain localisation in compression, evidenced in many other experimental programmes on concrete and rock,[7–11] suggests that, in the softening regime, energy dissipation takes place over an internal surface rather than within a volume, in close analogy with the behaviour in tension. These two interconnected phenomena may explain the size-scale effects on ductility. Owing to strain localisation, the post-peak branch of the stress–strain curve is no longer a true material property, but it becomes dependent on the specimen size and slenderness. Based on these experimental evidences, Hillerborg[12] and Markeset[13] proposed to model failure of concrete in compression (crushing) by means of strain localisation over a length proportional to the depth of the compressed zone, or defined as a material characteristic length.[14] In this way, the $\boldsymbol{\sigma}-\boldsymbol{\varepsilon}$ relationship used to describe the softening regime make it possible to address the issue of size effects, although the length over which the localisation occurs becomes a free parameter, usually defined by the best fitting of experimental data.

Based on the evidence that the post-peak dissipated energy referred to a unitary surface can be considered as a material parameter[7,10] and, consequently, that the post-peak stress–displacement relationship is independent of the specimen size,[8,9] Carpinteri *et al.*[15,16] and Corrado[17] have recently proposed modelling the process of concrete crushing using an approach analogous to the cohesive crack model,[18–21] which is routinely adopted for modelling the tensile behaviour of concrete. In tension, the localised displacement is represented by a crack opening, while in compression it would be represented by an interpenetration. This new approach, also based on the fracture mechanics concepts, is referred to as the overlapping crack model[15–17] and assumes a stress–displacement law as a material parameter for the post-peak behaviour of concrete in compression.

It is remarkable to note that, whereas the classic problem of uniaxial compression has received great attention from the scientific community, the state-of-the-art literature shows that only a few experimental studies have been proposed for the analysis of the mechanical behaviour of concrete in eccentric compression, and the related problem of size-scale effects is largely unsolved. The present paper introduces the mathematical aspects of the overlapping crack model for the description of concrete crushing in compression, exploring the analogies between tensile and compression tests. A new numerical algorithm is then proposed, based on the finite element method which is able to describe the non-linear behaviour of eccentrically loaded specimens in compression. This model is validated by means of a comparison between the numerical predictions and the results of the experimental tests carried out by Debernardi and Taliano.[22] Finally, using this model, the important issue of size-scale effects in eccentric compression is addressed, showing the limitations of the existing design formulae.

Overlapping crack model for the description of concrete crushing

In structural design, the most frequently adopted constitutive laws for concrete in compression describe the material behaviour in terms of stress and strain (elastic-perfectly plastic, parabolic-perfectly plastic, Sargin's parabola etc.). This approach, which implies an energy dissipation within a volume, does not permit the mechanical behaviour to be correctly described by varying the structural size. On the contrary, size-scale effects are attributable to strain localisation within one or more transversal or inclined bands.[2–6]

The present formulation adopts the stress–displacement relationship proposed by Carpinteri *et al.*[15,16] between the compression stress and the interpenetration, in close analogy with the cohesive model. The main hypotheses are detailed below.

(*a*) The constitutive law used for the undamaged material is a linear-elastic stress–strain relationship characterised by the values of the elastic modulus, E, the compression strength, $\boldsymbol{\sigma}_c$, and the ultimate elastic strain, $\boldsymbol{\varepsilon}_c$ (see Figure 1(a)).

(*b*) The crushing zone develops when the maximum compression stress reaches the concrete compression strength.

(*c*) The process zone is perpendicular to the principal compression stress.

(*d*) The damaged material in the process zone is assumed to be able to transfer a compression stress between the overlapping surfaces. Such stresses are assumed to be a decreasing function of the interpenetration, w^c (see Figure 1(b)). The following simple linear softening law can be used (see also the pioneering Hillerborg model[12]), although more complicated shapes could also be adopted

$$\boldsymbol{\sigma} = \boldsymbol{\sigma}_c \left(1 - \frac{w^c}{w^c_{cr}}\right) \tag{1}$$

where w^c is the interpenetration, w^c_{cr} is the critical value of the interpenetration corresponding to the condition of $\boldsymbol{\sigma} = 0$ and $\boldsymbol{\sigma}_c$ is the compression strength. The crushing zone is then represented by a fictitious overlapping, which is mathematically analogous to the fictitious crack in tension. It is important to note that, from the mathematical point of view, the overlapping displacement is a global quantity, and therefore it permits the structural behaviour to be characterised without the need for modelling the actual failure mechanism of the specimen into the details, which may vary from pure crushing to diagonal shear failure, to splitting, depending on its size-scale and slenderness.[5]

The proposed model, based on a fictitious interpenetration, permits a true material constitutive law to be obtained, independent of the structural size. This approach, in which the post-peak stress–displacement relationship is considered as a material constitutive law, is experimentally confirmed by van Vliet and van Mier[8] and by Jansen and Shah,[9] who considered specimens with different slenderness. Moreover, this assumption is more general, as it can be extended to specimens characterised by different sizes. To demonstrate this, the uniaxial compression tests carried out by Ferrara and Gobbi[23] on plain concrete specimens are considered. The slenderness varied from 0·5 to 2 and the scale range was 1:2:4. The experimental non-dimensional stress against average strain curves are shown in Figure 2(a), where S, M and L identify the three considered dimensions. As expected, the elastic

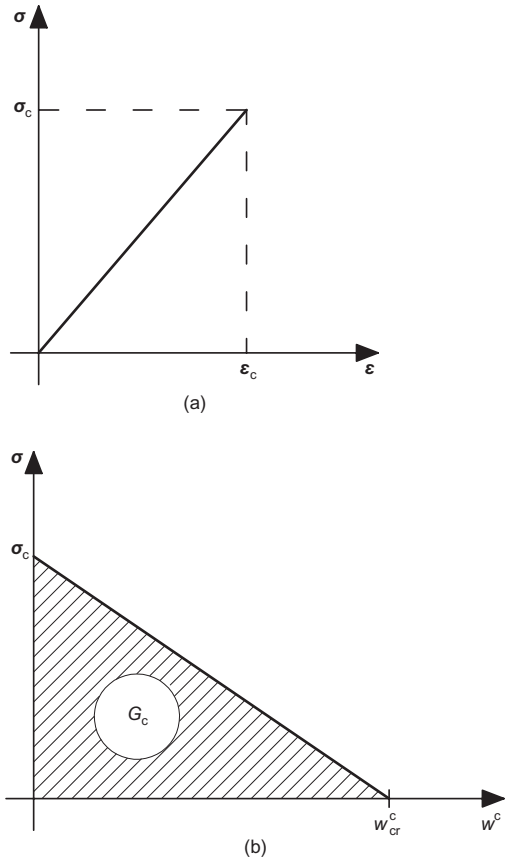

Figure 1. Double constitutive law introduced by the overlapping crack model for concrete in compression

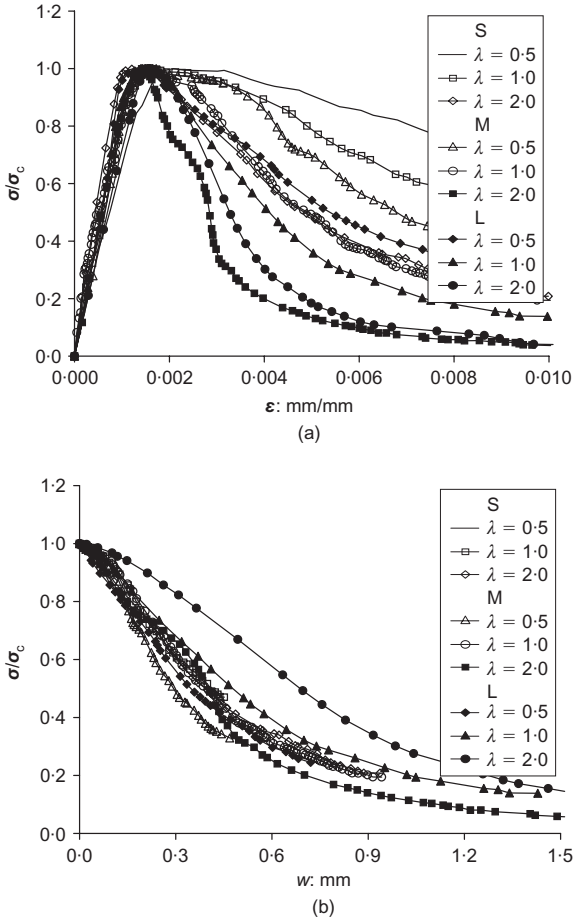

Figure 2. Uniaxial compression tests on specimens with different dimension and slenderness.[23] S, M and L denote, respectively, small, medium and large specimens. (a) $\boldsymbol{\sigma}$–$\boldsymbol{\varepsilon}$ relationship; (b) $\boldsymbol{\sigma}$–w post-peak relationship

behaviour is independent of any geometrical parameter, the slope of the corresponding branch being equal to the tangent elastic modulus of the material (Figure 2(a)). However, the post-peak behaviour is largely influenced by the slenderness and the scale of the specimen. As a consequence, the stress–strain relationship cannot be assumed as a material property. The stress–displacement curve for the softening regime can be obtained by computing the post-peak localised interpenetration through subtracting the elastic expansion, caused by the reduction of the applied stress in the post-peak regime, to the total shortening of the specimen (see Figure 2(b)). As a result of such an operation, the experimental stress–displacement curves related to specimens with different size or slenderness collapse onto a very narrow band, demonstrating that the $\boldsymbol{\sigma}-w$ relationship is able to provide a slenderness and size-scale independent constitutive law of concrete in compression.

It is worth noting that the crushing energy, G_C, defined as the area below the post-peak softening curve of Figure 1(b), is now a true material parameter, since it is not affected by the structural size. Dahl and Brincker[7] carried out a series of uniaxial compression tests with the aim of measuring the dissipated energy per unit cross-sectional area. They obtained values of about 50 N/mm and claimed that this dissipated energy becomes independent of the specimen size if the specimen is large enough. An empirical formulation for calculating the crushing energy has recently been proposed by Suzuki *et al.,*[10] based on the results of uniaxial compression tests carried out on plain and transversally reinforced concrete specimens. In the present study, the crushing energy is computed according to the aforementioned empirical equation, which considers the confined concrete compression strength by means of the stirrups yield strength and the stirrups volumetric content[10] (see Figure 3(a))

$$\frac{G_C}{\boldsymbol{\sigma}_c} = \frac{G_{C,0}}{\boldsymbol{\sigma}_c} + 10\,000\frac{k_a^2 p_e}{\boldsymbol{\sigma}_c^2} \tag{2a}$$

where $\boldsymbol{\sigma}_c$ is the average concrete compression strength, k_a is a parameter depending on the stirrups strength and volumetric percentage and p_e is the effective lateral pressure. The crushing energy for unconfined concrete, $G_{C,0}$, can be calculated using the following expression (see Figure 3(b))

$$G_{C,0} = 80 - 50k_b \tag{2b}$$

where the parameter k_b depends on the concrete compression strength.[10]

By varying the concrete compression strength from 20 to 90 MPa, Equation 2b gives a crushing energy ranging from 30 to 58 N/mm (Figure 3(b)). It is worth noting that $G_{C,0}$ is between two and three orders of magnitude higher than the tensile fracture energy, G_F, whereas the critical value for the overlapping

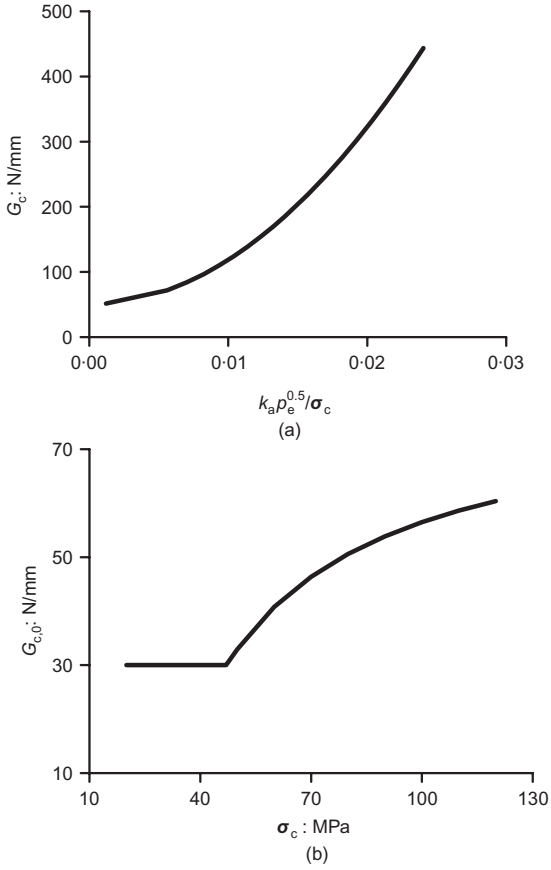

Figure 3. (a) Crushing energy against stirrups confinement; and (b) compression strength

displacement, $w_{cr}^c \approx 1$ mm, is one order of magnitude higher than the critical opening displacement in tension (see also the experimental results by Jansen and Shah[9]). Finally, it is noted that, in the case of concrete confinement, the crushing energy, computed using Equation 2a, and the corresponding critical value for crushing interpenetration, increase considerably (Figure 3(a)).

Uniaxial compression tests

According to the overlapping crack model, the mechanical behaviour of a plain concrete specimen subjected to uniaxial compression can be described by three simplified stages, analogously to the model proposed by Carpinteri[24] for concrete slabs in tension.

(*a*) The specimen behaves elastically without any damage or localisation zones, Figure 4(b). The displacement of the upper side is

$$\delta = \boldsymbol{\varepsilon} l = \frac{\boldsymbol{\sigma}}{E} l \quad \text{for } \boldsymbol{\varepsilon} \leqslant \boldsymbol{\varepsilon}_c \tag{3}$$

(*b*) After reaching the ultimate compression strength σ_c, the deformation starts to localise in a crushing band. The behaviour of this zone is described by

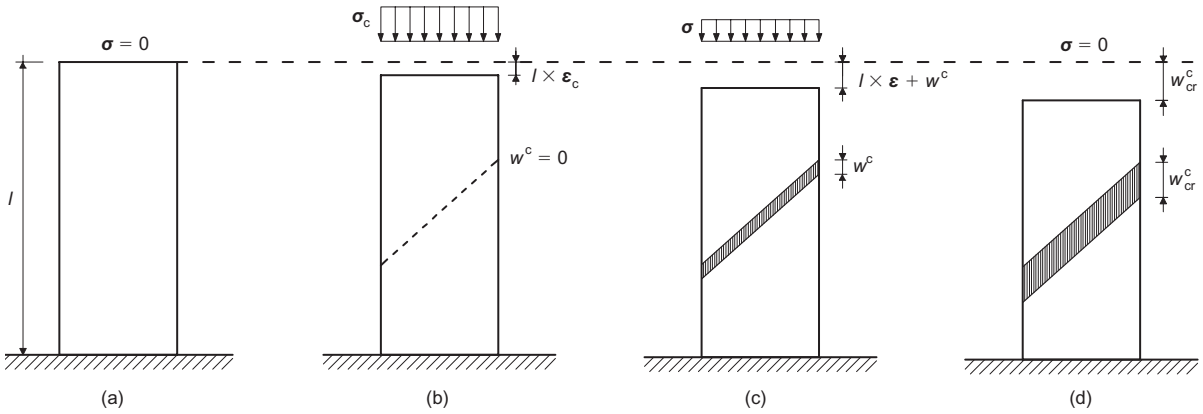

Figure 4. Subsequent stages in the deformation history of a specimen in compression

the softening law shown in Figure 1(b), whereas the outside part of the specimen behaves elastically, Figure 4(c). The displacement of the upper side can be computed as the sum of the elastic deformation and the interpenetration displacement w^c

$$\delta = \frac{\boldsymbol{\sigma}}{E} l + w^c \quad \text{for } w_c \leqslant w_{cr}^c \tag{4}$$

Introducing the softening law of Equation 1 into Equation 4, a one-to-one correspondence is obtained between δ and $\boldsymbol{\sigma}$

$$\delta = \frac{\boldsymbol{\sigma}}{E} l + w_{cr}^c \left(1 - \frac{\boldsymbol{\sigma}}{\boldsymbol{\sigma}_c}\right) \quad \text{for } w_c \leqslant w_{cr}^c \tag{5}$$

While the crushing zone overlaps, the elastic zone expands at progressively decreasing stresses. At this stage, the loading process will be stable if it is displacement-controlled, that is if the external displacement δ is imposed. However, this is only a necessary and not a sufficient condition for stability.

(*c*) When $\delta \geqslant w_{cr}^c$, concrete in the crushing zone is completely damaged and it is unable to transfer stresses, Figure 4(d). The compression stresses vanish and the condition of complete interpenetration (stage 3) becomes

$$\sigma = 0 \quad \text{for } \delta \geqslant w_{cr}^c \tag{6}$$

When $w_{cr}^c > \boldsymbol{\varepsilon}_c\, l$, the softening process is stable if it is displacement-controlled, because the slope $\mathrm{d}\boldsymbol{\sigma}/\mathrm{d}\delta$ at stage 2 is negative (Figure 5(a)). When $w_{cr}^c = \boldsymbol{\varepsilon}_c\, l$, this elementary model predicts an infinite slope and a sudden drop in the load bearing capacity under displacement control (Figure 5(b)). Finally, when $w_{cr}^c < \boldsymbol{\varepsilon}_c\, l$, the slope $\mathrm{d}\sigma/\mathrm{d}\delta$ of the softening branch becomes positive (snap-back), and a negative jump occurs, as shown in Figure 5(c).

Rearranging Equation 5

$$\delta = w_{cr}^c + \sigma \left(\frac{l}{E} - \frac{w_{cr}^c}{\sigma_c}\right) \tag{7}$$

The same conditions just obtained from a geometrical point of view (Figure 5), may also be given by the analytical derivation of Equation 7. Normal softening occurs for $\mathrm{d}\delta/\mathrm{d}\sigma < 0$, that is for

$$\frac{l}{E} - \frac{w_{cr}^c}{\boldsymbol{\sigma}_c} < 0 \tag{8}$$

whereas catastrophical softening (snap-back) occurs for $\mathrm{d}\delta/\mathrm{d}\sigma \geqslant 0$

$$\frac{l}{E} - \frac{w_{cr}^c}{\boldsymbol{\sigma}_c} \geqslant 0 \tag{9}$$

Equation 9 may be rearranged as follows

$$\frac{\left(w_{cr}^c/2b\right)}{\boldsymbol{\varepsilon}_c (l/b)} \leqslant \frac{1}{2} \tag{10}$$

where b is the specimen width.

The ratio $(w_{cr}^c/2b)$ is dimensionless and is a function of the material properties and of the structural size

$$s_E^c = \frac{w_{cr}^c}{2b} = \frac{G_C}{\boldsymbol{\sigma}_c b} \tag{11}$$

where $G_C = \frac{1}{2}\boldsymbol{\sigma}_c w_{cr}^c$ is the crushing energy (Figure 1(b)). The energy brittleness number in compression, s_E^c, analogous to that proposed by Carpinteri in 1984[20,25] for cohesive crack propagation in tension, describes the scale effects typical of fracture mechanics, that is the ductile–brittle transition when the size-scale increases. Equation 10 may be rewritten in the following form

$$\frac{s_E^c}{\boldsymbol{\varepsilon}_c \lambda} \leqslant \frac{1}{2} \tag{12}$$

where $\lambda = l/b$ is the specimen slenderness.

Therefore, when the size-scale and the specimen slenderness are relatively large and the crushing energy is relatively low, the global structural behaviour becomes brittle. The single values of parameters s_E^c, $\boldsymbol{\varepsilon}_c$ and λ are not responsible for the global brittleness or ductility of the structure considered, but only their combination $B = s_E^c/\boldsymbol{\varepsilon}_c \lambda$. When $B \leqslant \frac{1}{2}$, the concrete

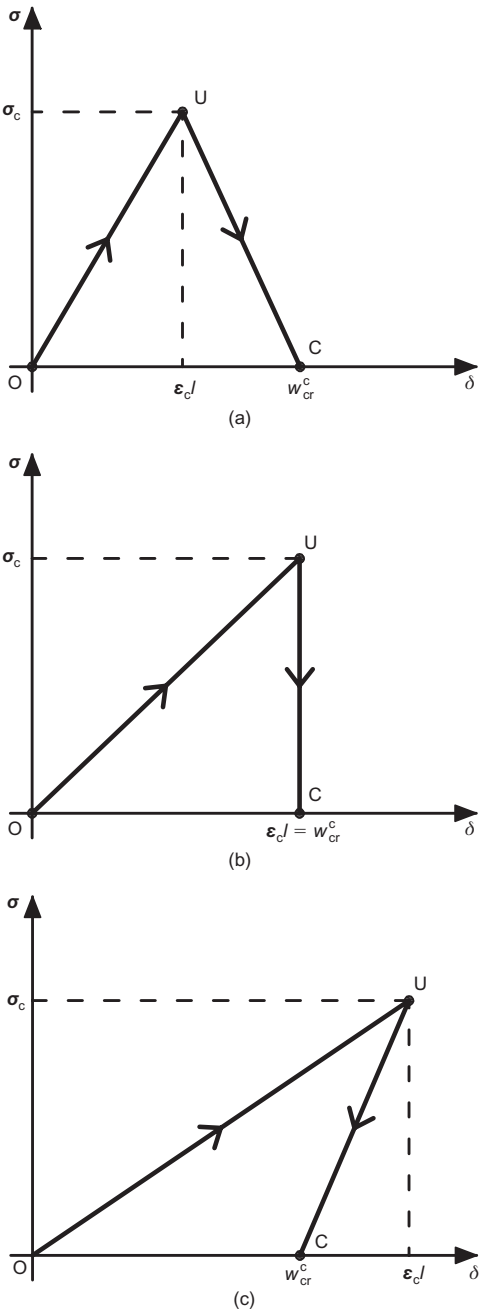

Figure 5. Stress–displacement response: (a) normal softening; (b) vertical drop; (c) catastrophic softening (snap back)

specimen of Figure 4 shows a mechanical behaviour which can be defined as brittle or catastrophic. In this case, a bifurcation of the global equilibrium occurs, since, when point U in Figure 5(c) is reached, the global unloading may occur along two alternative paths when the external displacement is decreased: the elastic UO or the virtual softening UC.

A more realistic simulation of concrete compression tests can be performed by introducing more sophisticated constitutive laws. In the following, in order to take into account the non-linear behaviour of concrete in the increasing branch, a well-known stress–strain

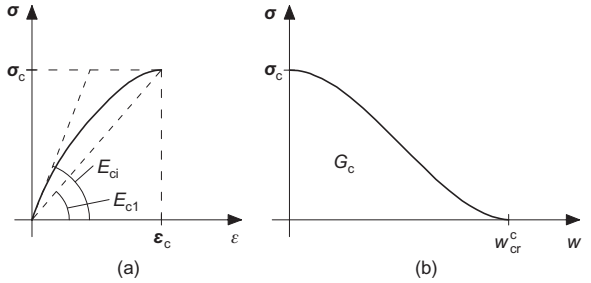

Figure 6. Improved constitutive laws for the overlapping crack model

relationship provided by the model code 90[26] is adopted up to the achievement of the concrete compression strength (see Figure 6(a))

$$\frac{\boldsymbol{\sigma}}{\boldsymbol{\sigma}_c} = \frac{(E_{ci}/E_{c1})(\boldsymbol{\varepsilon}/\boldsymbol{\varepsilon}_c) - (\boldsymbol{\varepsilon}/\boldsymbol{\varepsilon}_c)^2}{1 + [(E_{ci}/E_{c1}) - 2](\boldsymbol{\varepsilon}/\boldsymbol{\varepsilon}_c)} \tag{13}$$

where $\boldsymbol{\sigma}_c$ is the compression strength; $\boldsymbol{\sigma}$ is the actual value of the compression stress; $\boldsymbol{\varepsilon}$ is the compression strain; $\boldsymbol{\varepsilon}_c = -0{\cdot}0022$ ($\boldsymbol{\varepsilon}_{c1}$ in the original model code notation); E_{ci} is the tangent modulus; E_{c1} is the secant modulus from the origin to the peak compression stress, $\boldsymbol{\sigma}_c$. Moreover, the following stress–displacement cubic relationship describing the softening regime is introduced (see Figure 6(b)), which has been computed by imposing $\boldsymbol{\sigma} = \boldsymbol{\sigma}_c$ at $w^c = 0$, $\boldsymbol{\sigma} = 0$ at $w^c = w^c_{cr}$, and horizontal tangents in the same points

$$\frac{\boldsymbol{\sigma}}{\boldsymbol{\sigma}_c} = 2\left(\frac{w^c}{w^c_{cr}} + \frac{1}{2}\right)\left(1 - \frac{w^c}{w^c_{cr}}\right)^2 \tag{14}$$

A comparison between the numerical predictions obtained using Equations 13 and 14 and the experimental results of uniaxial compression tests carried out by Jansen and Shah[9] on specimens characterised by different slenderness and concrete strength are shown in Figures 7 and 8. Both experimentally and numerically it is possible to capture snap-back branches if a monotonic increasing function of time is assumed as the control parameter. Usually, the experimental tests are carried out using a circumferential displacement control (see Hudson *et al.*[11] and Jansen *et al.*[27]). However, this method is not suitable in the case of very slender specimen, as those shown in Figure 8, where the failure zone does not always develop in the middle of the specimen. For this reason, Jansen and Shah[9] adopted an alternative method, which is a linear combination of force and displacement, originally proposed by Okubo and Nishimatsu.[28] According to this method, a part of the elastic deformation is subtracted from the total specimen deformation, leaving the inelastic deformation as a stable feedback signal (for more details see Jansen and Shah[9]). Note that a similar approach is adopted in the proposed numerical procedure, where the overlapping displacement is the control parameter used to determine

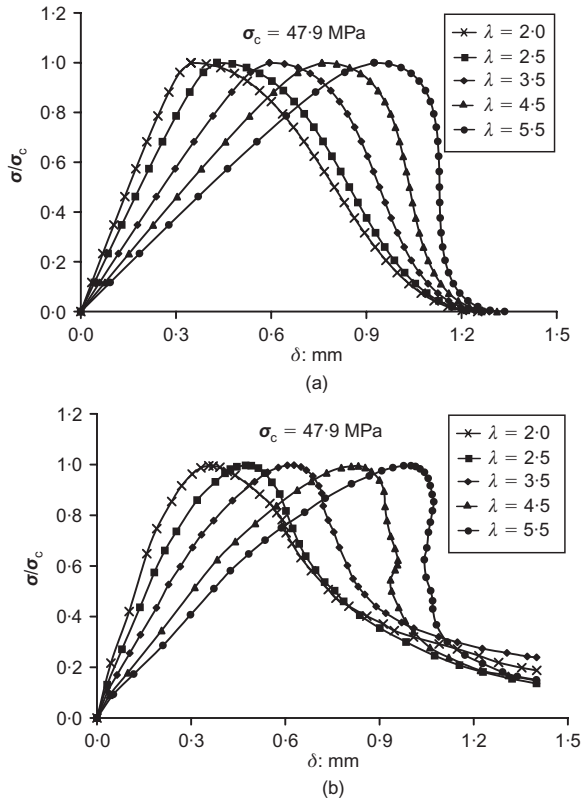

Figure 7. (a) Analytical and (b) experimental[9] non-dimensional stress against total shortening in the case of normal strength concrete. σ_c denotes the stress at the peak load

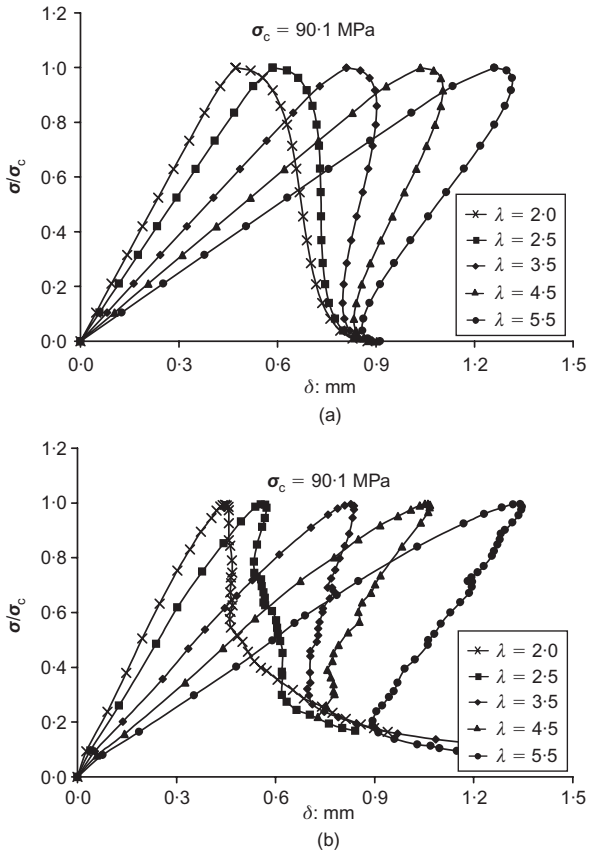

Figure 8. (a) Analytical and (b) experimental[9] non-dimensional stress against total shortening in the case of high strength concrete. σ_c denotes the stress at the peak load

$\boldsymbol{\sigma}$, according to Equation 1, and then δ, according to Equation 4.

The proposed numerical model, based on a more sophisticated relationship with respect to the linear one, exhibits a satisfactory prediction capability. In good agreement with the experiments, the mechanical behaviour becomes more brittle, with the appearance of snap-back instability by increasing the specimen slenderness and the concrete compression strength.

Eccentric compression tests

Description of the numerical algorithm

In this section, a simplified version of the numerical algorithm developed by Carpinteri *et al.*[16] describing the mechanical behaviour of RC beams in bending is presented in order to simulate the behaviour of plain concrete specimens subjected to eccentric compression by means of the overlapping crack model. In close analogy with the behaviour of concrete specimens subjected to uniaxial compression, all of the non-linear contributions in the post-peak regime are localised along the middle cross-section where interpenetration takes place, while the two half-specimens exhibit an elastic behaviour, as shown in Figure 9.

It is assumed that the stress distribution in the middle cross-section is linear-elastic until the maximum compression stress reaches the concrete compression strength. When this threshold is reached, concrete crushing is assumed to take place and a fictitious overlapping crack propagates towards the opposite vertical side of the specimen. Outside the overlapping zone, the material is assumed to behave linear-elastically. According to the overlapping crack model, the stresses in the overlapping zone are assumed to be a function of the amount of interpenetration and become equal to

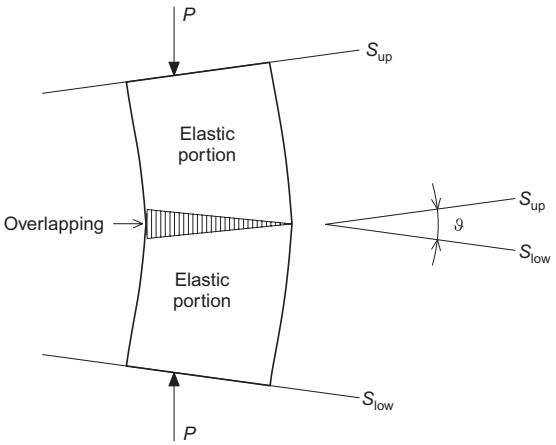

Figure 9. Idealisation of the specimen and definition of the total rotation

zero when the interpenetration is larger than the critical value w_{cr}^{c}, as shown in Figure 1(b). If the external force is applied outside the central core of inertia, the material behaviour on the tensile side is described by means of the well-known cohesive crack model.[25]

The middle cross-section of the specimen can be subdivided into finite elements by n nodes (Figure 10(a)). In this scheme, overlapping or cohesive stresses are replaced by equivalent nodal forces by integrating the corresponding pressures or tractions over each element size. Such nodal forces depend on the nodal closing or opening displacements according to the overlapping or cohesive softening laws.

The vertical forces, F, acting along such a cross-section can be computed as follows

$$\{\boldsymbol{F}\} = [\mathbf{K}_w]\{\boldsymbol{w}\} + \{\boldsymbol{K}_P\}P \tag{15}$$

where $\{\boldsymbol{F}\}$ is the vector of nodal forces, $[\mathbf{K}_w]$ is the matrix of the coefficients of influence for the nodal displacements, $\{\boldsymbol{w}\}$ is the vector of nodal displacements, $\{\boldsymbol{K}_P\}$ is the vector of the coefficients of influence for the applied force and P is the applied axial force. The coefficients of influence $[\mathbf{K}_w]$ have the physical dimension of a stiffness and are computed a priori with a finite element analysis by applying a unitary displacement to each of the nodes shown in Figure 10(a). In the generic situation shown in Figure 10(b), the following equations can be considered, taking into account the linear overlapping softening law (Equation 16a), the undamaged zone (Equation 16b) and the linear cohesive softening law (Equation 16c)

$$F_i = \boldsymbol{F}_c\left(1 - \frac{w_i^c}{w_{cr}^c}\right) \quad \text{for } i = 1, \ldots, (p-1) \tag{16a}$$

$$w_i = 0 \quad \text{for } i = p, \ldots, m \tag{16b}$$

$$F_i = \boldsymbol{F}_u\left(1 - \frac{w_i^t}{w_{cr}^t}\right) \quad \text{for } i = (m+1), \ldots, n \tag{16c}$$

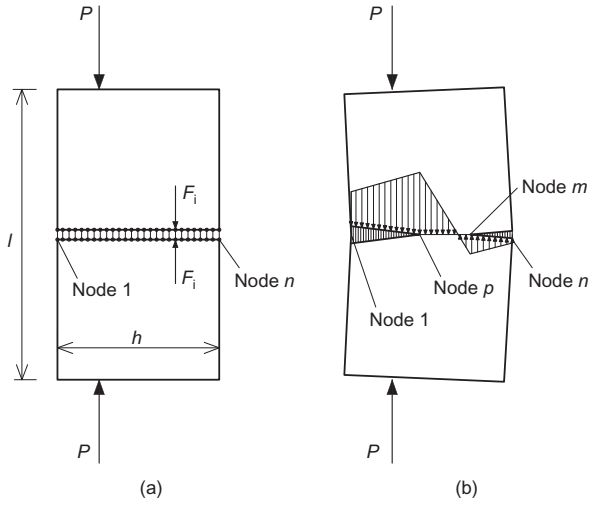

Figure 10. (a) Finite element nodes along the middle cross-section; (b) force distribution with cohesive crack in tension and overlapping crack in compression

Equations 15 and 16 constitute a linear algebraic system of $(2n)$ equations in $(2n+1)$ unknowns, namely $\{\boldsymbol{F}\}$, $\{\boldsymbol{w}\}$ and P. A possible additional equation can be chosen: it is possible to set either the force in the cohesive crack tip, m, equal to the ultimate tensile force, or the force in the overlapping crack tip, p, equal to the ultimate compression force. In the numerical scheme, the situation which is closer to one of these two possible critical conditions is chosen. This criterion will ensure the uniqueness of the solution on the basis of physical arguments. The driving parameter of the process is the position of the crack tip that the considered step has reached in the limit resistance. Only this tip is moved when passing to the next step.

In close analogy with contact mechanics, where the area of contact is unknown *a priori* and has to be determined using a non-linear numerical control scheme, in the present work the extension of the overlapping zone in eccentric bending tests has to be determined iteratively for each value of the applied load. However, a main difference with contact mechanics is that the equilibrium solution to be found in the current problem is governed by the stress-overlapping displacement in Equation 1 instead of by the Signorini-Fichera boundary conditions (see Wriggers[29] and Paggi *et al.*[30]).

Finally, at each step of the algorithm, it is possible to calculate the specimen rotation, ϑ, defined in Figure 9 as follows

$$\vartheta = \{\boldsymbol{D}_w\}^T\{\boldsymbol{w}\} + D_P P \tag{17}$$

where $\{\boldsymbol{D}_w\}$ is the vector of the coefficients of influence for the nodal displacements, with physical dimensions of $[\mathrm{L}]^{-1}$, and D_P is the coefficient of influence for the applied force with physical dimensions of $[\mathrm{F}]^{-1}$.

Comparison between model predictions and experimental results

In this section, the comparison between the numerical predictions and the experimental results of the testing programme by Debernardi and Taliano[22] on 15 plain concrete specimens subjected to eccentric compression is carried out. The dimensions of the specimens, shown in Figure 11(a), were kept constant, whereas five different degrees of eccentricity were considered, varying between 0 and 48 mm. The mean value of the compression strength, determined on ten cubes with 6 cm sides, was equal to 56 N/mm^2, with standard deviation of 3·5 N/mm^2. In order to reduce the influence of the boundary conditions due to friction between the specimen and the loading platens, the deformations were measured in the central part of the specimen, which was further subdivided into three parts. The positioning of the measuring instruments, shown in Figure 11(b), with particular regard to the devices 3–8, permits the deformations of three portions of the specimen to be evaluated, each one having a length of 112 mm. The most important aspects of the experi-

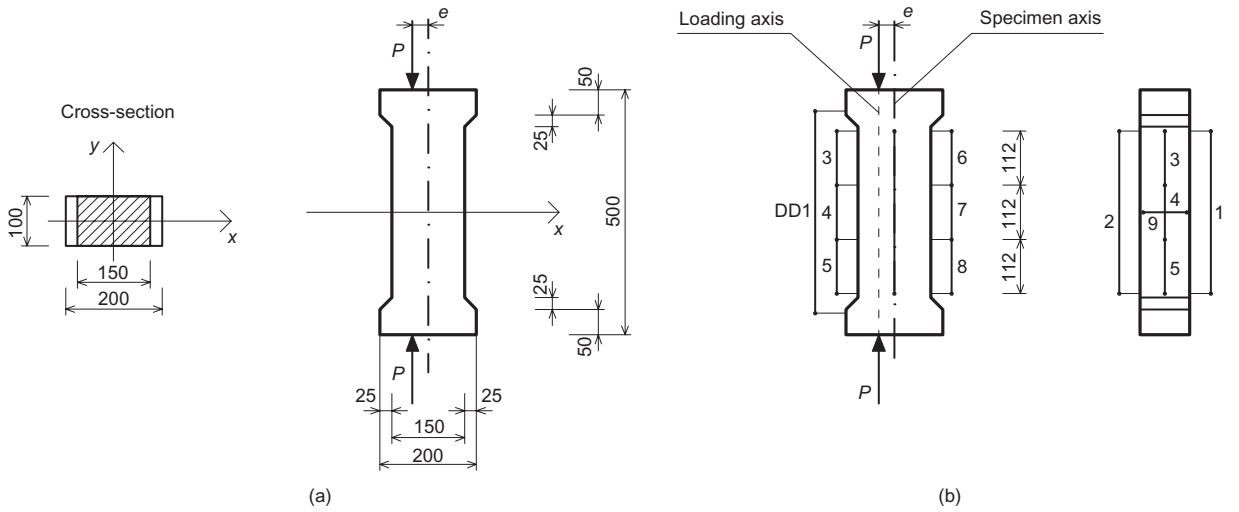

Figure 11. Eccentric compression tests[22]: typical specimen dimensions (a); arrangement of the measuring instruments (b)

ments were the correct positioning of the specimen and the application of the load at a predetermined level of eccentricity. Both extremities of the specimen were confined by means of special stirrups to prevent the opening of longitudinal cracks. The servo-hydraulic testing machine operated in strain-controlled conditions by applying a load such that the deformation in the most compressed fibres, measured by means of the DD1 gauge, increased at a constant rate up to failure. By this procedure, the softening stage until failure can be followed after the achievement of the peak load.

As a result of the experiments, the applied load and the deformation, Δl, recorded by the several extensometers related to the length l, were acquired. The rotations of each part of the specimen can be computed as

$$\vartheta_i = \frac{(\Delta l_{left} - \Delta l_{right})}{h} \tag{18}$$

where h is the distance between two measuring bases opposite to each other.

Hence, the total rotation of the analysed specimens, with a length equal to 336 mm, is given by the sum of the rotations of the three portions. It is worth noting that, by subdividing the total length of the specimen into three parts, a localisation of deformations in the central part has been put into evidence.

The length of the specimens assumed for the simulations is equal to $l = 336$ mm, as the length of the specimen supplied with the measuring devices in the testing programme (see Figures 10 and 11). In the numerical scheme, the middle cross-section of the concrete specimen is discretised into 100 finite elements and the coefficients of influence entering Equation 15 are preliminarily determined using the finite element method.

The experimental tests are also simulated by means of the stress–strain relationships provided by the model code 90[26] for modelling concrete in compression. In particular, Equation 13 is adopted to describe the whole increasing branch of the stress–strain diagram and the first part of the descending branch for values of $|\boldsymbol{\sigma}|\boldsymbol{\sigma}_c \geqslant 0{\cdot}5$, or, equivalently for $|\boldsymbol{\varepsilon}| \leqslant \boldsymbol{\varepsilon}_{c,lim}$. For $|\boldsymbol{\varepsilon}| > \boldsymbol{\varepsilon}_{c,lim}$, the descending branch of the $\boldsymbol{\sigma}$–$\boldsymbol{\varepsilon}$ diagram has to be described by the following equation

$$\boldsymbol{\sigma} = \left[\left(\frac{1}{\boldsymbol{\varepsilon}_{c,lim}/\boldsymbol{\varepsilon}_c} \xi - \frac{2}{\left(\boldsymbol{\varepsilon}_{c,lim}/\boldsymbol{\varepsilon}_c\right)^2} \right) \left(\frac{\boldsymbol{\varepsilon}}{\boldsymbol{\varepsilon}_c} \right)^2 + \left(\frac{4}{\boldsymbol{\varepsilon}_{c,lim}/\boldsymbol{\varepsilon}_c} - \xi \right) \frac{\boldsymbol{\varepsilon}}{\boldsymbol{\varepsilon}_c}^{-1} \right] \boldsymbol{\sigma}_c \tag{19}$$

with

$$\xi = \frac{4\left[\left(\boldsymbol{\varepsilon}_{c,lim}/\boldsymbol{\varepsilon}_c\right)^2 \left[\left(E_{ci}/E_{c1}\right) - 2\right] + 2\left(\boldsymbol{\varepsilon}_{c,lim}/\boldsymbol{\varepsilon}_c\right) - \left(E_{ci}/E_{c1}\right)\right]}{\left[\left(\boldsymbol{\varepsilon}_{c,lim}/\boldsymbol{\varepsilon}_c\right)\left[\left(E_{ci}/E_{c1}\right) - 2\right] + 1\right]^2} \tag{20}$$

The values of E_{ci}, E_{c1} and $\boldsymbol{\varepsilon}_{c,lim}$ are given in Table 2.1.7. of the model code 90[26] for different values of concrete compression strength.

In the application of Equations 13, 19 and 20, it was assumed that all the cross-sections have the same behaviour, and that the total rotation is given by multiplying the curvature of one of these sections for the specimen height.

The numerical results are compared with the experimental ones in the P–ϑ diagrams for different eccentricities (see Figure 12). First, it is worth noting that, except the case of $e = 12$ mm, a perfect agreement is obtained between the numerically predicted and the experimentally evaluated softening branches, confirming the good prediction capability of the proposed model, in spite of the simple linear softening relationship adopted. Moreover, the numerical model captures the experimentally observed decrement of the maximum applied load due to the contemporaneous presence of bending moment and axial force. The discrepancy between the numerical and the experimental curves in the

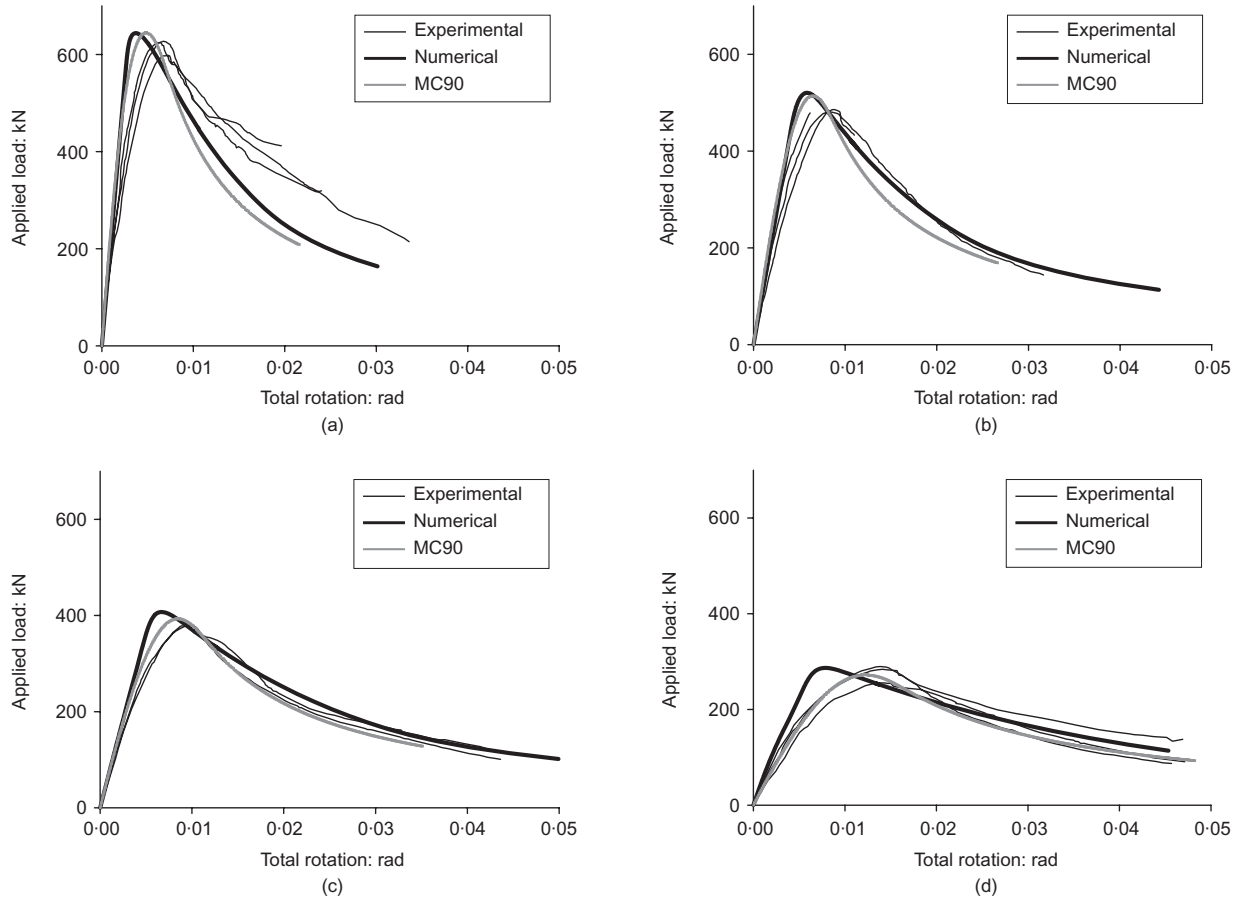

Figure 12. Numerical and experimental applied load against total rotation diagrams for the specimens tested by Debernardi and Taliano,[22] by varying the eccentricity: (a) e = 12 mm; (b) e = 24 mm; (c) e = 36 mm; (d) e = 48 mm

increasing branch suggests that a more complex constitutive law, with a non-linear contribution, should be considered instead of the linear-elastic one, in order to improve the description of the real behaviour. Finally, a general good agreement is evidenced between the curves obtained by the application of the constitutive law provided by model code 90 (dashed lines in Figure 12) and the experimental results. This agreement is probably owing to a coincidence, because, as shown in the next section, the real behaviour of the specimens is scale-dependent, whereas model code 90 predictions completely disregard the size-scale effects.

Size-scale and slenderness effects in eccentric compression tests

In this section, a study of the size-scale and slenderness effects on the behaviour of concrete prisms subjected to eccentric compression is presented. To this aim, three different structural sizes, characterised by cross-section dimensions, $b \times h$, equal to 50×75, 100×150, 200×300 mm, and three different slendernesses, $\lambda = 1{\cdot}0$, $2{\cdot}2$, $4{\cdot}0$, are considered. Besides, the following four values of eccentricity are explored: $e = 0{\cdot}08h$, $e = 0{\cdot}16h$, $e = 0{\cdot}24h$, $e = 0{\cdot}32h$. Unfortunately, it is impossible to carry out a direct numerical against experimental comparison owing to the lack of experimental data in the literature.

The size-scale effects, for different slendernesses and for an eccentricity equal to $0{\cdot}16h$, are shown in the non-dimensional applied load versus total rotation curves of Figure 13. It is worth noting that, independently of the prism slenderness, the post-peak mechanical behaviour is size-scale dependent. In particular, the softening regime exhibits a ductile-to-brittle transition by increasing the specimen size for a constant slenderness. Furthermore, the value of the maximum applied load results to be a slightly decreasing function of the structural size. As mentioned before, from Figure 13 it is deduced that the constitutive law provided by model code 90, which assumes an energy dissipation within a volume, does not capture the size-scale effects. It is interesting to note that, in the case of $\lambda = 1{\cdot}0$, model code 90 curve is very close to the behaviour of the smallest specimen (Figure 13(a)). In the case of $\lambda = 2{\cdot}2$, it agrees with the response of the intermediate specimen (Figure 13(b)), whereas for $\lambda = 4{\cdot}0$ it is close to that of the largest one (Figure 13(c)).

The effect of slenderness is investigated in the non-dimensional load against total rotation diagram of Figure 14 for a given specimen size (cross-section equal to 100×150 mm) and a given eccentricity ($e = 0{\cdot}08h$).

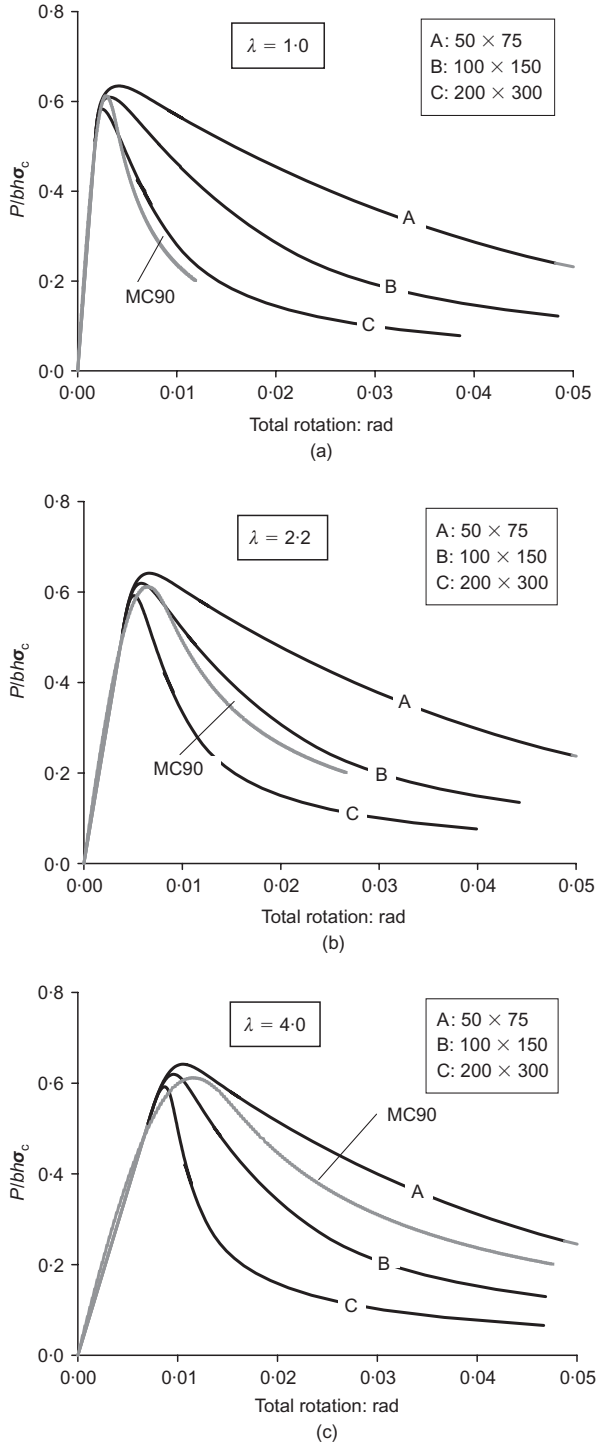

Figure 13. Numerically predicted size-scale effects by varying the specimen slenderness and for a given load eccentricity $e = 0{\cdot}16h$

As expected, the stiffness of the elastic branch is a decreasing function of the slenderness, since it is proportional to the specimen height. Correspondingly, little increment of the softening slope is evidenced.

The effect of the load eccentricity is shown in Figure 15 for $\lambda = 2{\cdot}2$ and cross-section dimensions equal to 100×150 mm. The increment in the eccentricity, e, produces a reduction in the stiffness of the elastic

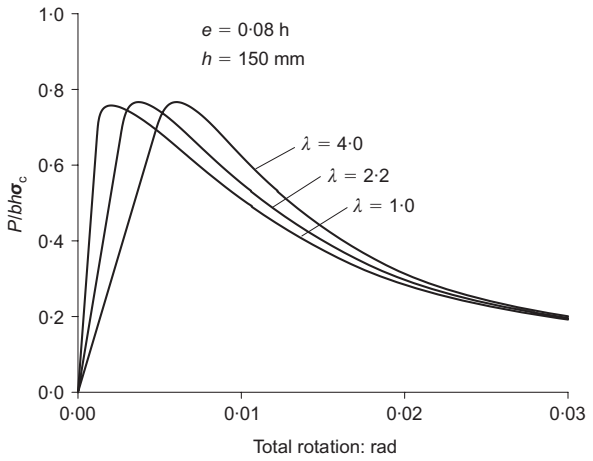

Figure 14. Numerically predicted non-dimensional applied load against total rotation curves for specimens with different slenderness

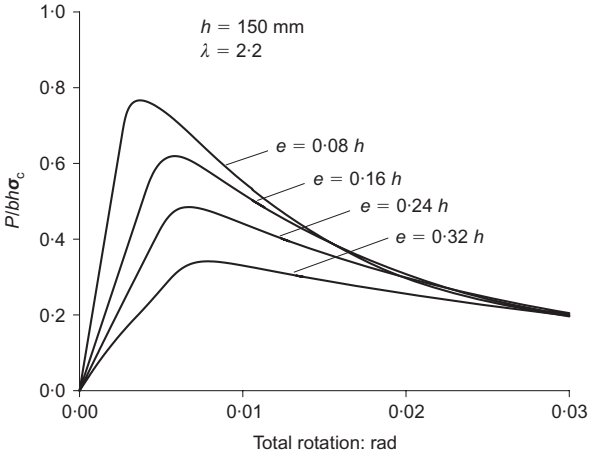

Figure 15. Numerically predicted non-dimensional load against total rotation curves for given specimen dimension and slenderness and different load eccentricity

branch, owing to the increase in the bending moment. At the same time, the mechanical behaviour becomes undoubtedly more ductile. This result puts into evidence the important contribution on ductility of the post-peak regime of concrete in compression in the case of high strain gradient, as, for example, in a reinforced concrete column subjected to an eccentric axial force.

Finally, the non-dimensional load against total rotation curves for different values of the brittleness number in compression, s_E^c, defined by Equation 11, are shown in Figure 16. The values of the slenderness and the eccentricity are, respectively, equal to 4 and $0{\cdot}08h$. Specimens characterised by the same value of s_E^c exhibit the same mechanical behaviour. A ductile-to-brittle transition is observed by decreasing the brittleness number from 0·0686 to 0·0006. This transition can be obtained either by increasing the specimen dimension, b, or by increasing the compression strength, $\boldsymbol{\sigma}_c$, or by

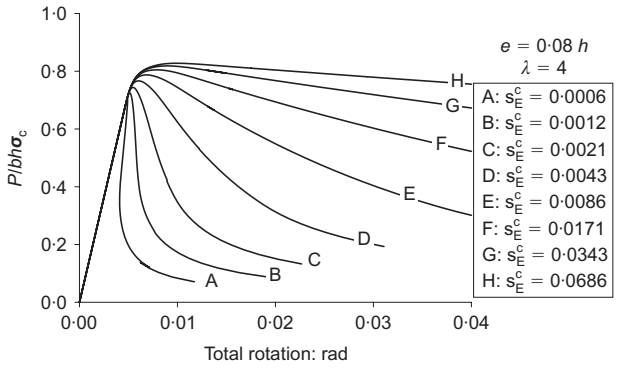

Figure 16. Numerically predicted non-dimensional applied load against total rotation diagrams by varying the energy brittleness number in compression, s_E^c

decreasing the crushing energy, G_C. In the case of large structural dimensions and very low crushing energy, a catastrophic failure (snap-back) is obtained, as clearly evidenced by curve A in Figure 16.

Conclusion

In the present paper, a theoretical model and a numerical algorithm have been proposed for the analysis of the mechanical behaviour of concrete specimens subjected to uniaxial or eccentric compression tests. The concept of overlapping crack in compression, which is analogous to the cohesive crack in tension, makes it possible synthetically to characterise the mechanical response of quasi-brittle materials in compression without simulating each specific failure mode. In fact, when the slenderness decreases, a transition from splitting to crushing collapse takes place in reality. A similar transition can occur by varying the size-scale of the element. In spite of this, the use of a global quantity, represented by the overlapping crack displacement, has the advantage that it defines a true size- and slenderness-independent constitutive law. The good agreement between the analytical predictions and the experimental results in the case of uniaxial compression tests demonstrates the reliability of the proposed approach (see Figures 7 and 8).

Moreover, from the dimensional analysis point of view, it is remarkable to note that neither the individual values of the crushing energy, the compression strength nor the specimen size are responsible for the ductile-to-brittle transition in the mechanical response, but rather only their function s_E^c, which defines an energy brittleness number in compression analogous to that proposed in tension by Carpinteri in 1984.[20]

As far as the numerical simulations of eccentric compression tests are concerned, the use of the extension of the fictitious crushing zone and the length of the tensile crack as the driving parameters is highly effective, as it follows the descending branch of the load-rotation diagram with either negative or positive slope (see Figure 16). From the structural point of view, is has been shown that the peak load is a decreasing function of the load eccentricity (see Figure 15). More importantly, the structural ductility, evaluated as the area below the load against total rotation diagram, turns out to be a decreasing function of the specimen size, for given values of slenderness and load eccentricity (see Figure 13). This sheds a new light on the size-scale effects in eccentric compression tests, which are completely disregarded by the design formula proposed by model code 90.

References

1. Bažant Z. P. and Xiang Y. Size effect in compression fracture: splitting crack band propagation. *Journal of Engineering Mechanics, ASCE*, 1997, **123**, No. 2, 162–172.
2. Carpinteri A., Ferro G. and Monetto I. Scale effects in uniaxially compressed concrete specimens. *Magazine of Concrete Research*, 1999, **51**, No. 3, 217–225.
3. Reunion Internationale des Laboratoires et Experts des Materiaiux, Systemes de Construction et Ouvrages (RILEM) Technical Committee 148-SSC. Strain-softening of concrete in uniaxial compression. *Materials and Structures*, 1997, **30**, No. 4, 195–209.
4. Indelicato F. and Paggi M. Specimen shape and the problem of contact in the assessment of concrete compressive strength. *Materials and Structures*, 2008, **41**, No. 2, 431–441.
5. Carpinteri A., Ciola F. and Pugno N. Boundary element method for the strain-softening response of quasi-brittle materials in compression. *Computers and Structures*, 2001, **79**, No. 4, 389–401.
6. van Mier J. G. M. *Strain Softening of Concrete under Multiaxial Compression*. PhD thesis, Eindhoven University of Technology, The Netherlands, 1984.
7. Dahl H. and Brincker R. Fracture energy of high-strength concrete in compression. *Fracture of Concrete and Rock: Recent Developments*. *Proceeding of the International Conference on Recent Developments in the Fracture of Concrete and Rock*, Cardiff, Wales, 1989, pp. 523–536.
8. van Vliet M. and van Mier J. Experimental investigation of concrete fracture under uniaxial compression. *Mechanics of Cohesive-Frictional Materials*, 1996, **1**, No. 1, 115–127.
9. Jansen D. C. and Shah S. P. Effect of length on compressive strain softening of concrete. *Journal of Engineering Mechanics*, 1997, **123**, No. 1, 25–35.
10. Suzuki M., Akiyama M., Matsuzaki H. and Dang T. H. Concentric loading test of RC columns with normal- and high-strength materials and averaged stress-strain model for confined concrete considering compressive fracture energy. *Proceedings of the 2nd fib Congress*, *Naples*, 2006, ID 3–13 (on CD-ROM).
11. Hudson J. A., Brown E. T. and Fairhurst C. Shape of the complete stress–strain curve for rock. *Proceedings of the 13th Symposium on Rock Mechanics*, *University of Illinois, Urbana*, *Illinois*, 1971, 773–795.
12. Hillerborg A. Fracture mechanics concepts applied to moment capacity and rotational capacity of reinforced concrete beams. *Engineering Fracture Mechanics*, 1990, **35**, No. 1–3, 233–240.
13. Markeset G. and Hillerborg A. Softening of concrete in compression: localization and size effects. *Cement and Concrete Research*, 1995, **25**, No. 4, 702–708.
14. Bažant Z. P. Identification of strain-softening constitutive relation from uniaxial tests by series coupling model for localization. *Cement and Concrete Research*, 1989, **19**, No. 6, 973–977.
15. Carpinteri A., Corrado M., Paggi M. and Mancini G. Cohesive versus overlapping crack model for a size effect analysis of

RC elements in bending. *Fracture Mechanics of Concrete Structures. Proceedings of the 6th International FraMCoS Conference, Catania*, 2007, **2**, 655–663.
16. Carpinteri A., Corrado M., Paggi M. and Mancini G. A numerical approach to modelling size effects on the flexural ductility of RC beams. *RILEM Materials and Structures*. doi: 10·1617/s11527–008–9454–y.
17. Corrado M. *Effetti di scala sulla capacità di rotazione plastica di travi in calcestruzzo armato*. PhD thesis, Politecnico di Torino, Torino, 2007, in Italian.
18. Hillerborg A., Modeer M. and Petersson P. E. Analysis of crack formation and crack growth in concrete by means of fracture mechanics and finite elements. *Cement and Concrete Research*, 1976, **6**, No. 6, 773–782.
19. Petersson P. E. *Crack growth and development of fracture zones in plain concrete and similar materials*. Lund Institute of Technology, 1981. Technical report, LUTVDG/TVBM-1006
20. Carpinteri A. Interpretation of the Griffith instability as a bifurcation of the global equilibrium. *Application of Fracture Mechanics to Cementitious Composites*, *Proceedings of a NATO Advanced Research Workshop*, Evanston, USA, 1984, pp. 287–316.
21. Carpinteri A. Cusp catastrophe interpretation of fracture instability. *Journal of the Mechanics and Physics of Solids*, 1989, **37**, No. 5, 567–582.
22. Debernardi P. G. and Taliano M. Softening behaviour of concrete prisms under eccentric compressive forces. *Magazine of Concrete Research*, 2001, **53**, No. 4, 239–249.
23. Ferrara G. and Gobbi M. E. *Strain Softening of Concrete under Compression*. ENEL-CRIS Laboratory, Milano, Italy, 1995. Report to RILEM Committee 148-SSC.
24. Carpinteri A. Snap-back and hyperstrength in lightly reinforced concrete beams. *Magazine of Concrete Research*, 1988, **40**, No. 145, 209–215.
25. Carpinteri A. Size effects on strength, toughness, and ductility. *Journal of Engineering Mechanics*, *ASCE*, 1989, **115**, No. 7, 1375–1392.
26. Comité Euro-International du Béton. *CEB–FIP Model Code 1990*. Thomas Telford, Lausanne. CEB Bulletin No. 213/214, 1993.
27. Jansen D. C., Shah S. P. and Rossow E. C. Stress–strain results of concrete from circumferential strain feedback control testing. *ACI Materials Journal*, 1995, **92**, No. 4, 419–428.
28. Okubo S. and Nishimatsu Y. Uniaxial compression testing using a linear combination of stress and strain as the control variable. *International Journal of Rock Mechanics and Mineral Science and Geomechanics,* 1985, **22**, No. 5, 323–330.
29. Wriggers P. *Computational Contact Mechanics*. Wiley, Chichester, 2002.
30. Paggi M., Carpinteri A. and Zavarise G. A unified interface costitutive law for the study of fracture and contact problems in heterogeneous materials. *Analysis and Simulation of Contact Problems. Lecture Notes in Applied and Computational Mechanics* (Wriggers P. and Nackenhorst U. (eds)). Springer Verlag, Berlin, 2006, Vol. 27, pp. 297–304.

Discussion contributions on this paper should reach the editor by 1 May 2010